Computer Simulation of the Ionic Atmosphere around Z-DNA

J. L. F. Abascal,*,† M. Domercq,‡ and J. C. Gil Montoro†

Departamento de Química-Física, Facultad de Ciencias Químicas, Universidad Complutense, 28040 Madrid, Spain, and I.E.S. Tierno Galván, 28914 Leganés, Spain

Received: July 4, 2006; In Final Form: September 28, 2006

We describe a coarse-grained model for Z-DNA that mimics the DNA shape with a relatively small number of repulsive interaction sites. In addition, negative charges are placed at the phosphate positions. The ionic atmosphere around this grooved Z-DNA model is then investigated with Monte Carlo simulation. Cylindrically averaged concentration profiles as well as the spatial distribution of ions have been calculated. The results are compared to those for other DNA models differing in the repulsive core. This allows the examination of the effect of the DNA shape in the ionic distribution. It is seen that the penetrability of the ions to the DNA groove plays an important role in the ionic distribution. The results are also compared with those reported for B-DNA. In both conformers the ions are structured in alternating layers of positive and negative charge. In Z-DNA the layers are more or less concentric to the molecular axis. Besides, no coions enter into the single groove of this conformer. On the contrary, the alternating layers of B-DNA are also structured along the axial coordinate with some coions penetrating into the major groove. In both cases we have found five preferred locations of the counterions and two for the coions. The concentration of counterions reaches its absolute maximum at the narrow Z-DNA groove and at the minor groove of B-DNA, the value of the maximum being higher in the Z conformer.

I. Introduction

The biological role of DNA lies ultimately in its physicochemical properties which relate DNA structure and function.[1,2] Although this fact alone would justify the interest in the physics and chemistry of DNA, the peculiarities of DNA make it an interesting molecule by itself. Since in solution the phosphates are ionized, DNA is a highly charged and stiff polyion due to repulsion between the charged phosphates (the persistence length is about 150−200 base pairs[2]). In this way, DNA is a paradigm of a polyelectrolyte system. As a consequence of the electrostatic field created by the high charge density of DNA, the molecule is surrounded by a cloud of counterions. Small angle neutron scattering[3] and NMR experiments[4] provide strong evidence for a layer of bound counterions intimately associated with DNA. The condensation of ions and the calculation of the ionic distribution around DNA is a challenging physical problem.[5−10] An interesting phenomenon is that of the charge inversion in which the coion concentration exceeds that of the counterions at a certain distance to the polyion. Usually associated to the charge inversion one finds that of the polyion charge is overneutralized at those distances. The phenomenon has been reported for concentrated solutions of 1:1 electrolytes and dilute solutions of 2:2 electrolytes in the vicinity of a charged wall.[11,12] Charge inversion was also observed in integral equation studies[13] and simulations[14] of 2:2 electrolytes around a polyion. Experimentally, it has been observed in electrophoresis of other strong polyelectrolytes.[15] Although the first observation of overneutralization in DNA with added 1:1 salt was in a computer simulation work,[16] the modified Poisson−Boltzmann theory also predicts the charge inversion for concentrated electrolyte solutions.[10] The importance of the overneutralization in DNA is that it may explain the condensation of DNA mediated by the counterions[17−20] or the approach to DNA of negatively charged molecules. The simulations of DNA also showed that much lower concentrations were required for the occurrence of the overneutralization in the presence of multivalent counterions.[21] Sophisticated theoretical approximations also account for the DNA overneutralization in solutions containing multivalent counterions.[9,10,22−24]

Another salt-induced effect is the conformational change from B- to Z-DNA. Although the idea of a left-handed DNA helix has been around for some time, it was not until 1972 that Pohl and Jovin demonstrated the existence of Z-DNA.[25] Quite surprisingly, the first crystal DNA structure solved by X-ray diffraction was not the expected Watson−Crick right-handed structure but a left-handed helix.[26] As the phosphate groups are placed describing a zigzag line, this left-handed DNA conformer was called Z-DNA. There are now strong indications that Z-DNA may play an important biological role because the altered conformation of DNA can have tremendous implications in gene expression and host response to viruses.[27−30] As Z-DNA is thinner than B-DNA, its charged phosphates are closer to each other giving stronger repulsions among them so that B is, in principle, the most stable DNA form. The transition from B- to Z-DNA then requires a stabilization of the Z form with respect to the B form by means of extrinsic effects. Among these, most of the experimental studies have been focused on supercoiling[31,32] and salt effects.[25,33] Due to the great complexity of the problem, few theories have been applied to the dependence on salt concentration of the relative stability of the B and Z forms of DNA. Besides, the theoretical treatments have been forced to use simplified models for the system components (polyion,

* Address correspondence to this author.
† Universidad Complutense.
‡ I.E.S. Tierno Galván.

10.1021/jp064199z CCC: $33.50 © 2006 American Chemical Society
Published on Web 11/16/2006

water, and ions) and the interactions between them. The initial approaches were based on the Poisson−Boltzmann (PB) equation and a homogeneously charged hard cylinder model of polyelectrolytes.[34−36] More recently, results have been obtained for relatively more complex DNA models and theories.[37−40] On the other hand, it has been shown that the discretization of the charges in the ionic structure around charged planes and rods can cause enhanced localization of the counterions near the surface.[41,42] This can be important in the modelization of DNA. Interestingly, theoretical treatments based in models that consider only the spatial arrangement of charged phosphates (a double helical chain) give a more or less satisfactory account of experimental data on the B- to Z-DNA transition despite the simplicity of the underlying model[43−45] (in fact using the size of the ions as an adjustable parameter the agreement with experiment is excellent). These findings have been confirmed by computer simulation results[46,47] although a similar agreement with experiment is found for more elaborate (coarse-grained) DNA models with no adjustable ion size parameters.[48]

We have shown in the previous paragraphs two examples of salt-induced effects on DNA. In both cases the changes in DNA are determined by changes in the ionic atmosphere around the polyion. This topic has been the subject of several reviews.[49,50] In fact, this issue is so important that the ionic distribution is the target property of many theoretical and simulation studies irrespective of whether they are used as a necessary step in the calculation of other DNA properties. The more recent theories for the calculation of the ionic atmosphere in polyelectrolytes have reached a considerable degree of sophistication.[9,10,51−53] In fact, the computer cost is so high that several problems (as the B- to Z-DNA transition) are out of the reach of these theories except for very simple models. Computer simulation is also costly but it has the advantage that its results are, in principle, exact (see the recent review by Lyubartsev[54] on molecular simulations of DNA counterion distribution). The level at which DNA is described may be quite different. Interesting contributions have been based on a full atomistic representation, on a charged rod, or even on a simple pair of charged helical lines.[45] A number of results already have been reported for the ionic atmosphere around atomistic DNA models.[55−65] The atomistic approach is probably necessary for the analysis of the mechanism of the conformational transitions in DNA, but it could be a waste of computer time for the thermodynamics of this or other problems as the thermal denaturation of DNA.[66] Besides, an adequate sampling of the ionic atmosphere is difficult because the ions get kinetically trapped for long times—of the order of about 10 ns in some binding sites as the minor groove of B-DNA.[63] For these reasons, the need for a mesoscopic modeling of DNA is gaining an increasing acceptance.[67−70] In this work we will use a mesoscopic representation to calculate the ionic distribution around Z-DNA by computer simulation. The main feature of the model is that it mimics the DNA grooved structure while retaining a considerable degree of simplicity. We may benefit from the experience in the development of a similar model for B-DNA.[16] In fact, the grooved model for B-DNA has been successfully employed by the authors to calculate the spatial distribution of ions around B-DNA,[71] to analyze the competition between multivalent and monovalent counterions,[21] and to investigate the thermodynamics of the B- to Z-DNA transition.[48,72,73] Other research groups have also used the grooved B-DNA model in different contexts[20,74−77] (notice that these authors sometimes refer to it as the Montoro−Abascal Model, MAM).

Compared with the huge number of papers devoted to B-DNA, the literature about computer simulation of Z-DNA is rather scarce. Most of the works are related to the stability[78−81] and hydration[79,82,83] of Z-DNA with use of classical simulation, but it should be noted an investigation of the electronic structure with use of first principles simulation.[84] To our knowledge, there are no computer simulation studies of the ionic distribution around Z-DNA. Also scarce are the theoretical studies of the spatial distribution of ions around Z-DNA.[38,85,86] In this work we intend to contribute to this issue. The goal of this paper is then 2-fold. First we propose a coarse-grained model for Z-DNA that allows a cost-effective computer simulation of Z-DNA with explicit ions. On the other hand, we want to use the model to investigate the condensation of ions around Z-DNA and compare it with that obtained for B-DNA and with that obtained for other Z-DNA models. Although a deep investigation of the origin of the salt-induced B- to Z-DNA transition is out of the scope of this work, we expect that this study can be a step in that direction.

TABLE 1: Parameters for the Generation of the Phosphate Positions in Z-DNA[a]

s	p	$\rho_0^{(s,p)}$	$\phi_0^{(s,p)}$	$z_0^{(s,p)}$
1	1	7.31	0.0	0.00
2	1	7.31	164.0	0.03
1	2	6.27	115.4	1.70
2	2	6.27	348.6	5.76

[a] s refers to the different complementary chains and p to the type of phosphates within each chain. Radial and axial coordinates (ρ, z) are given in Å while the angular coordinates (ϕ) are expressed in deg.

II. Z-DNA Models

In this work we will use several models for Z-DNA. When choosing a model there is always a tradeoff between two requirements. One wants models as realistic and also as simple as possible. As the discretization of the DNA charge may have an important effect in the condensation of counterions around DNA,[41,42] the extremely simple representation of the DNA charge by a homogeneously charged rod is not satisfactory for our purposes. Thus, for all of the models employed in this work, unity charges (in electrons) are placed at the phosphate positions in canonical Z-DNA. There are two different Z-DNA conformers (usually denoted as Z_I and Z_{II}[87]) but the relevant one for the B- to Z-DNA transition is the first one. In Z_I there are two nonequivalent phosphate positions and, thus, the repeating unit is a pair of dimers. There are 6 repeating units per turn which makes a total of 24 nucleotides per turn. The elevation and rotation per repeating unit are 7.43 Å and 60°, respectively. Thus, the coordinates of the phosphates are specified by[87]

$$\rho_i^{(s,p)} = \rho_0^{(s,p)}$$

$$\phi_i^{(s,p)} = \phi_0^{(s,p)} - 60 \cdot i$$

$$z_i^{(s,p)} = z_0^{(s,p)} + 7.43 \cdot i \qquad (1)$$

where $i = 0, ..., 5$ accounts for the six repeating units along one helix turn. The parameters $\rho_0^{(s,p)}$, $\phi_0^{(s,p)}$, and $z_0^{(s,p)}$ are the radial, angular, and axial coordinates (in a cylindrical reference system) of the reference phosphate. There are two complementary chains $s = 1, 2$ and the superscript $p = 1, 2$ refers to the nonequivalent phosphate positions of the repeating unit. The generation of all the phosphate coordinates requires four sets of values for the different originating phosphates. These are given in Table 1. The height of the helix turn is then 44.58 Å.

Since it contains 24 phosphates, Z-DNA gives a smaller linear charge density than B-DNA (20 phosphates for a helix turn of 33.80 Å).

The phosphates are not only the center of electrostatic interactions but also the origin of a soft repulsive potential. In our model they interact through a Ramanathan−Friedman (RF) potential

$$U^{\mathrm{RF}}(r_{ij}) = \frac{A_{\mathrm{M}} e^2 |z_i z_j|}{4\pi\epsilon N_{\mathrm{c}} n} (r_{\mathrm{i}} + r_{\mathrm{j}})^{(n-1)} \frac{1}{r_{ij}^{\,n}} \qquad (2)$$

where $A_{\mathrm{M}} = 1.7476$ is the Madelung constant for the halite structure, $N_{\mathrm{c}} = 6$ is the coordination number for that structure, $n = 9$ is a parameter controlling the steepness of the repulsive potential, and r_i, r_j are parameters determining the size of ions i and j. The RF functionality has been traditionally used for ion−ion interactions. In this way, we assimilate all the charge−charge interactions irrespective of whether the charged particles are mobile ions or polyelectrolyte sites. Besides, in this work we use the same size parameter for anions, cations, and phosphates. In particular, the value $r_i = 1.4214$ Å has been chosen as it gives bulk electrolyte properties approximately corresponding to a restricted primitive model with hard-sphere diameters of 4.2 Å.[88] This size has been widely used in electrolyte solution studies[14,89−92] and roughly corresponds to a sodium ion on account of its hydration shell.[90,93]

In the so-called "empty" Z-DNA model, the soft repulsive spheres located at the phosphate positions are the only repulsive interactions between DNA and the solution ions. As commented above, successful theoretical approaches are implicitly based on the "empty" model as the underlying physical representation of DNA in solution.[43−45]

The repulsive core is different in the other models used in this work. The phosphate charges may be simply embedded in a repulsive cylinder. The repulsive potential is a soft interaction defined by the equation

$$U^{\mathrm{rep,poly}}(\rho_p) = K_2^{\mathrm{rep}} \frac{1}{(\rho_p - \rho_0)^9} \qquad (3)$$

where $K_2^{\mathrm{rep}} = 2.7291 \times 10^{-17}$ J·Å^9 and ρ_{p} is the ion−polyelectrolyte distance. From the two possible values for ρ_0 (see Table 1) it seems convenient to use the radial coordinate of the more external one, i.e., $\rho_0 = 7.31$ Å. The model will be denoted as the discretely charged soft repulsive (DS) model. Notice that the DS model does not conform to the grooved DNA shape. The main consequence is that the counterions cannot accumulate within the grooves and are forced to be outside the repulsive cylinder.

The repulsive envelope of the third model tries to mimic as close as possible the DNA shape. For this reason it is a grooved model, and since it is made with simple elements we call it a *grooved primitive* (GP) model. We have proceeded for Z-DNA in a similar manner as for the development of the grooved primitive model for B-DNA.[16] By making several cuts to Richard's surface of the all-atom representation of Z-DNA we obtained an average section that was fitted with a number of geometrical elements. As we try to keep the similarity with the GP model of B-DNA, we place a spherical repulsive center at the phosphates coordinates with the same diameter used for B-DNA. The bases were represented in B-DNA by means of a repulsive cylinder. This is not possible for Z-DNA because this conformer has the molecular axis shifted with respect to the position of the bases. In fact, Z-DNA has a single groove but it is so deep that it almost reaches the molecular axis (see Figure 1).

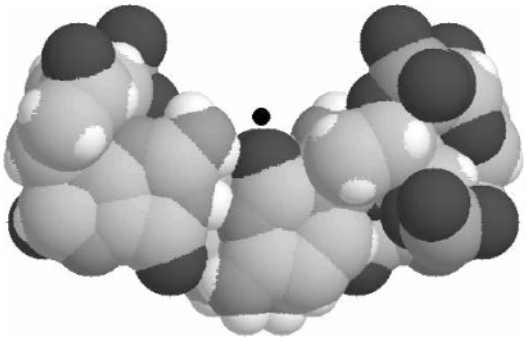

Figure 1. Representation of a guanine-cytosine·cytosine-guanine tetranucleotide in Z-DNA. The black circle marks the position of the molecular axis.

We have represented the bases of a dinucleotide as a repulsive site shifted with respect to the molecular axis. The interaction of these spheres is also a repulsive RF potential (eq 2) but with a different size. The radius of these sites, $r_i = 2.64$ Å, corresponds to a hard sphere diameter of about 7.8 Å, the same as the cylinder diameter in B-DNA. The radial coordinate of the sites representing the bases is 3.9 Å to make it tangent to the polyelectrolyte axis, as can be observed in Figure 1. Finally, to close the accessible space between the bases and the phosphates we put there an additional repulsive interaction site. These intermediate spheres are identical with the phosphate sites except that they do not carry charge. In other words, they also interact through the Ramanathan−Friedman potential with the same radius as the phosphate sites. The position of these intermediate interaction sites is chosen so that they are in the line between the phosphates and the spheres representing the bases (i.e., the z coordinate is just that of the contiguous phosphate). The exact point is determined such that the phosphate−base distance is 1.54 times the base−intermediate site distance. In summary, the grooved Z-DNA model is made up of 24 charged phosphate groups (which are also repulsive centers), 24 intermediate repulsive sites sized as the phosphates, and 12 larger repulsive sites (each one representing a base-pair) per helix turn.

A transversal section of the model is shown in Figure 2. The schematic plot corresponds to a helical projection onto the plane of a reference phosphate. Taking as a reference a $p = 1$ phosphate, the coordinates of the interaction sites for a pair of dinucleotides (the repeating unit in Z-DNA) are given in Table 2. Figure 3 represents one helix turn of the Z-DNA grooved model. The phosphates show the well-known left-handed helix with the phosphates forming a zigzag line. It should also be noticed that the GP model reproduces the single deep groove of Z-DNA. Notice finally that consecutive bases overlap considerably and are not aligned so the ensemble of these sites forms an internal helix around the molecular axis.

Figure 4 presents the accessible volumes of B- and Z-DNA calculated with the probe-sphere algorithm[94] for a probe sphere of 1.6 Å (see ref 16 for a discussion of the accessible volume for a B-DNA GP model). More specifically, Figure 4 displays the differential element of the nonaccessible volume to the probe. In this way, a straight line gives the element of volume $2\pi\rho h$ for the cylinder with radius ρ and height h. The slope of the curves is then proportional to the height of the helix, and it is thus greater for Z-DNA than for B-DNA. In summary, the area below the curves at a given radial coordinate indicates the

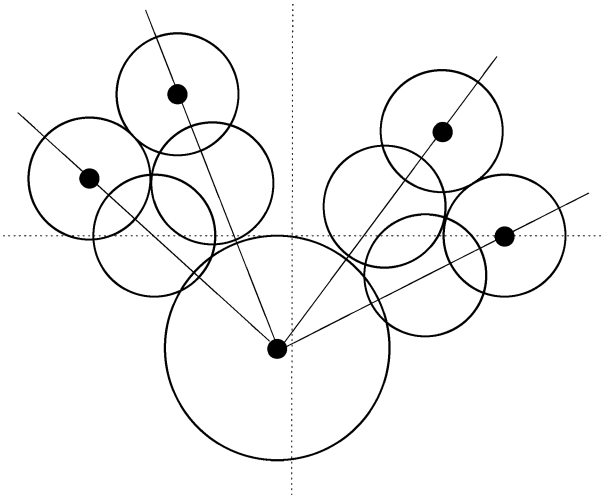

Figure 2. Transversal section of the grooved Z-DNA model helically projected onto the plane of the rightmost phosphate. The phosphate positions have been marked with small filled circles. The single groove is at the upper part of the figure. Notice also that the base sphere is tangent to the molecular axis.

TABLE 2: Coordinates of the Interaction Sites for a Pair of Dinucleotides in the GP Model of Z-DNA[a]

	coordinates			
site	ρ	ϕ	z	distance to the bases
base	3.90	262.0	0.00	0.00
phosphate, $p = 1$	7.31	0.0	0.00	8.75
intermediate	4.76	343.5	0.00	5.68
phosphate, $p = 1$	7.31	164.0	0.03	8.75
intermediate	4.76	180.5	0.03	5.68
base	3.90	232.0	3.72	0.00
phosphate, $p = 2$	6.27	115.4	1.70	9.38
intermediate	3.30	132.9	1.70	6.09
phosphate, $p = 2$	6.27	348.6	5.76	9.38
intermediate	3.30	331.0	5.76	6.09

[a] Distances (as well as the ρ and z coordinates) are given in Å and ϕ is in deg.

volume inaccessible to the ions while the area between the curves and the straight lines gives the accessible volume. The grooved B-DNA model has an internal cylindrical core which, as can be seen in Figure 4, prevents completely the entrance of ions. After the discontinuity, the increase of the inaccessible volume is almost independent of ρ. This means that the accessible/nonaccessible volume ratio decreases. In other words, for distances larger than the radius of bases there is a net increase of space available for counterions in DNA. This reflects a relatively important accessibility of the ions to the B-DNA grooves. For Z-DNA, the spheres of the bases behave essentially as a repulsive cylinder with minor deviations indicating that the single groove cannot accommodate easily the probe sphere. The differential volume increases with the radial coordinate closely following the straight line. At a distance close to the radial coordinate of the phosphates, the inaccessible volume attains a maximum and, afterward, it drops down abruptly. This is consistent with the idea of Z-DNA as a thinner and more inaccessible structure than B-DNA.

III. The Simulations

We have performed Monte Carlo simulations of Z-DNA models with added monovalent salt and implicit solvent. The effect of the solvent is included through its relative dielectric constant for which we used the value 78.36 corresponding to water at 25 °C. The ionic concentrations are those relevant for the B−Z transition. It is known that some DNA sequences may experience the transition even at physiological salt concentrations[95] while for other sequences the required salt concentration may reach values of about 5.4 M.[96] As our models are sequence-independent we have to choose specific values representative of the conditions for which the more stable form is the B and Z form, respectively. In particular, we will examine the results at approximately 1 and 4.3 M salt concentration. Because of the high ionic concentration and (as we will see below) the existence of a boundary with bulk concentrations, the inhomogeneity along the simulation box is relatively small compared to that of simulations with the cell model and no added salt. Thus we may employ classical Metropolis sampling. About 30 000 cycles were used for the complete equilibration period (a cycle means as many single-particle moves as the number of mobile ions). The number of cycles in the production phase was 40 000. The simulated states are given in Table 3.

The simulation of systems with explicit electrostatic charges requires some care because of the long-range extent of the

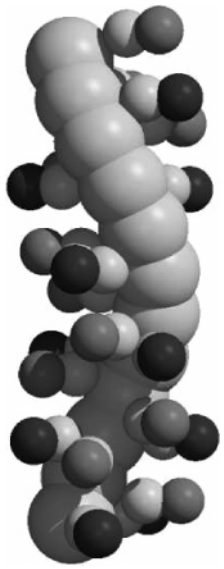

Figure 3. Grooved primitive model for Z-DNA. The two distinct types of phosphates are depicted with a slightly different intensity. Notice the zigzag arrangement of phosphates, the single (very deep) groove, and the helical shape of the ensemble of the spheres representing the bases.

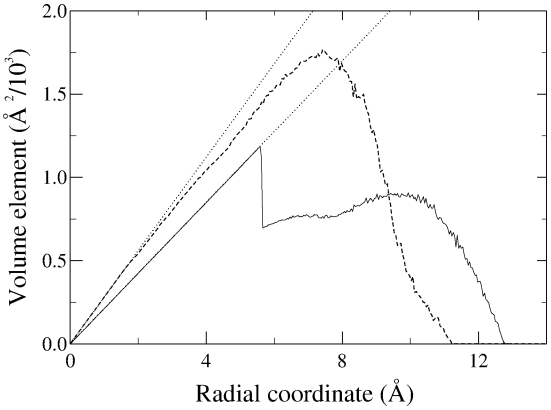

Figure 4. Differential elements of the volume nonaccessible to a probe (with a 1.6 Å radius) for a complete helix turn of the Z-DNA and B-DNA grooved models (dashed and solid line, respectively). The dotted straight lines are the corresponding volume elements for cylinders with radii equal to the radial coordinate and the same height as the Z-DNA and B-DNA helix turn, respectively.

TABLE 3: Simulations of This Work[a]

	C^{bulk} (M)		no. of ions			geometry (Å)			
form	nominal	actual	N_{n+}	N_+	N_-	L	R^I	Ap	r_c
				"empty" model					
B	1.0	0.99	40	195	195	67.6	32.5	39.2	13.0
Z	1.0	0.97	48	256	256	89.2	32.5	39.1	13.0
Z	4.5	4.31	24	265	265	89.2	22.5	26.7	8.0
				DS model					
B	1.0	0.95	40	310	310	67.6	36.0	50.3	13.0
Z	1.0	0.95	48	370	370	89.2	34.4	47.8	13.0
Z	4.5	4.27	24	280	280	89.2	24.4	28.6	8.0
				GP model					
B	1.0	0.99	40	205	205	67.6	32.5	40.4	13.0
Z	1.0	0.99	48	256	256	89.2	32.5	39.1	13.0
Z	4.5	4.50	24	265	265	89.2	22.5	26.7	8.0

[a] As the final bulk concentrations differ slightly from the nominal (intended) ones we write down both values though we will refer always in the text to the nominal concentrations. N_{n+} is the number of ions needed to cancel the polyion charge, and N_+ and N_- are the number of cations and anions of the added salt. L is the axial length of the simulation box, and R^I, Ap, and r_c are the parameters of the MBFB method for the radial boundary conditions (see the text and ref 98).

forces. The use of more or less standard techniques as the usual three-dimensional Ewald sums is inappropriate as we do not want the polyion to interact with its replicas. The geometry of the problem (a long polyion immersed in a solution of counterions and coions) imposes a clear difference between a singular orientation (that of the polyion) and those perpendicular to it. Then, an alternative procedure could be the explicit calculation of the electrostatic interactions within the simulation box and to approximate the polyion segments outside the simulation cell by uniformly charged lines. Unfortunately, it has been proven that this simple procedure is inaccurate.[41] In our case, the polyion is rigid and the charges are placed with a periodicity determined by the helix pitch. Thus, we can make use of an exact formula that gives the interaction between an ion and an infinitely long array of discrete charges

$$U_{i\nu}^{\text{array,inf}}(\rho_{i\nu},\Delta z_{i\nu}) = 2z_i\lambda_B b_\nu^{-1}\beta^{-1}[\log(\rho_{i\nu}) - 2\sum_{j=1}^{\infty} K_o(\kappa_j\rho_{i\nu})\cos(\kappa_j z_{i\nu})] \quad (4)$$

where $\rho_{i\nu}$ is the distance from the ion to the array ν, $\lambda_B = e^2\beta/(4\pi\epsilon)$ [the Bjerrum length], b_ν is the distance between two consecutive charges along the array, $\kappa_j = 2\pi j/b_\nu$, $\Delta z_{i\nu}$ is the axial coordinate of the ion with respect to the closest charged site of the array, and K_o is the modified Bessel function of order zero and second kind. The first term is the potential of an infinite homogeneous line of charge and the second is the charge discreteness contribution. The total potential between the charges in an infinite DNA helix and a mobile ion is then

$$U_{ip}^{\text{sites},\infty} = \sum_\nu U_{i\nu} \quad (5)$$

The long-range correction due to the potential created by the mobile ions outside the simulation cell has been calculated by using the radial density profile. The justification for this is that the ionic charge density profile in the axial direction is not as inhomogeneous as that of the polyelectrolyte because the charged sites of the latter are kept fixed while the ions are mobile and, thus, undergo thermal fluctuations which reduce the inhomogeneity.

As for the periodicity along the plane perpendicular to the molecular axis it is well-known that the effect of the polyion charge extends up to a certain distance. Beyond that point one finds the same concentration for counterions and coions, the bulk salt concentration c_{bulk}. Accordingly, a hard boundary could seem appropriate but the presence of the boundary results in a spurious attractive potential.[97] We have used the modulated bulk as a fuzzy boundary method[98] (MBFB). In this method, the cylinder corresponding to the cell model (the inhomogeneous region) is immersed in a periodic box (a hexagonal prism in our case) filled with bulk solution and the hard wall removed, so that mobile ions are able to cross the boundary. The ions interact with the surrounding bulk through a discrete particle−particle modulated (short-ranged) Coulomb potential[99] while the missing tail is recovered as a mean field contribution computed in a self-consistent way. In this way our simulations correspond to an infinitely long DNA chain at infinite dilution with added salt of bulk concentration c_{bulk}.

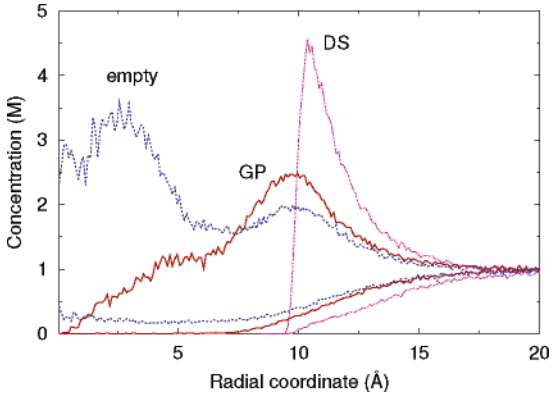

Figure 5. Concentration profiles around Z-DNA at 1 M salt concentration for the grooved model (GP), discretely charged with a cylindrical soft repulsive (DS) model and "empty" model. The upper curves are for counterions and the bottom ones for coions.

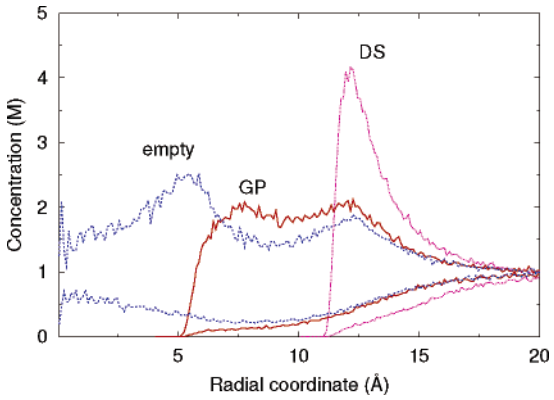

Figure 6. Concentration profiles around B-DNA at 1 M salt concentration. The results for the GP and DS models have been taken from ref 16.

IV. Results

In this section we present the ionic distribution around Z-DNA for the "empty", DS (soft cylinder), and GP (grooved) models. To compare the results for both DNA conformers, we will also include here some results for B-DNA.

1. Cylindrically Averaged Concentration Profiles. The concentration profiles around Z-DNA and B-DNA at 1 M salt concentration are shown in Figures 5 and 6, respectively. Given the high electrostatic field of both conformers, the counterions approach the phosphates and, depending on the available space, penetrate into the grooves. In this way, the concentration profile of the counterions reflects the accessibility to the grooves.

Let us first compare the results for the grooved Z- and B-DNA models. The characteristic double-hump in B-DNA (also appearing in all-atom simulations[100]) does not appear in Z-DNA. The calculations of Misra and Honig[38] using the PB equation for an atomistic model also show a double maximum in the counterions profile for B-DNA but not for the Z conformer. For the latter, our simulations yield a single and sharp maximum at 10 Å and a small plateau at 5 Å. The maximum occurs closer to the molecular axis than the second maximum of B-DNA, which appears at 12 Å. This is consistent with the position of the phosphates in both conformers (see Table 1). Another consequence of the different molecular arrangement is the presence of a small number of counterions adjacent to the molecular axis in the grooved Z-DNA model (recall that the sites representing the bases are slightly shifted from the axis). The coincidence of the internal repulsive core of the B-DNA model with the molecular axis makes impossible the presence of counterions at small radial coordinates, in particular, for $\rho < 5$ Å. Finally, it is surprising that the maximum concentration of counterions is slightly higher in Z-DNA than in B-DNA (2.5 vs. 2.1 M, respectively) despite the lower linear charge density of the former. But notice that the width of the single peak in Z-DNA is much more reduced than the extended double-maximum of B-DNA. A further analysis on this point is delayed until we discuss the neutralization of the DNA charge. The tails of the counterion concentration profiles are similar for Z- and B-DNA beyond 15 Å from the axis. The same holds for the coion profiles. Perhaps the influence of the polyelectrolyte charge extends a little bit longer in B-DNA: at 20 Å there is still a small difference in the concentration profiles of counterions and coions while for Z-DNA the profiles have already converged to the bulk concentration at such distance. As for the coions, the concentration profiles in Figures 5 and 6 indicate that the coions do not enter significantly into the grooves of the Z-DNA GP model. In fact, the concentration is null for radial distances smaller than 7 Å. This is a larger value than that for the grooved B-DNA model for which some coions may appear as close as 5 Å from the DNA axis. As shown above, there is no significant difference in the tails of the coion profiles of both DNA forms.

The maximum observed in the GP models counterions profile—at 10 and 12 Å for Z- and B-DNA, respectively—also appears at a similar distance to the axis in the "empty" DNA models (Figures 5 and 6). But now, the absence of a repulsive barrier enables a deeper entrance of counterions and hence the appearance of a second maximum close to the molecular axis. This is consistent with the double maximum in B-DNA, though the first peak is now shifted toward the molecular axis. For Z-DNA, the small hump of the GP model at 5 Å transforms into an independent peak in the "empty" model (shifted toward the molecular axis as in B-DNA). The first maximum has a higher counterion concentration than the second one, the difference between the height of the peaks being more important in Z-DNA than in B-DNA. Besides, the existence of an extended positively charged region makes possible the presence of some coions in the internal region of the "empty" Z- and B-DNA models. In fact, the concentration of coions is far from negligible at $\rho = 0$. Although in both conformers c_{coion} is close to 0.5 M, the ratio $c_{counterion}/c_{coion}$ is markedly larger for B-DNA at the molecular axis. At large distances from the polyion, the concentration profiles for the "empty" models are increasingly convergent with those of the GP models for both B-DNA and Z-DNA.

With regard to the DS model, the concentration profiles are substantially different from those for the GP and "empty" models. In contrast with the differences between models, the concentration profiles of the DS models are very similar in both DNA forms. The presence of a repulsive cylinder in B-DNA or the large radius of the sites representing the bases in Z-DNA lead to a very sharp peak in the counterions profile. The height of the peak is slightly over 4 M in both conformers. At larger distances, the counterion concentration decreases in an exponential-like manner while the coions profile is a slowly increasing monotonic function. The reported results for B-DNA[16] show that the overall shape of the counterion and coion concentration profiles are remarkably similar to that of a homogeneously charged rod. This indicates that the discretization of the charges by itself is not sufficient to provide a qualitatively distinct behavior. Only when it is coupled with the accessibility of the counterions to the grooves does one obtain qualitatively distinct concentration profiles. In other words, when the counterions are not allowed to enter into the grooves, they feel essentially a strong linear charge density but they are not specially sensitive to the spatial details of the charge distribution of the polyion. But when the ions can enter into the grooves, the concentration profiles are determined by both the spatial distribution of the DNA charges and the DNA shape (see also Figure 10 of ref 16).

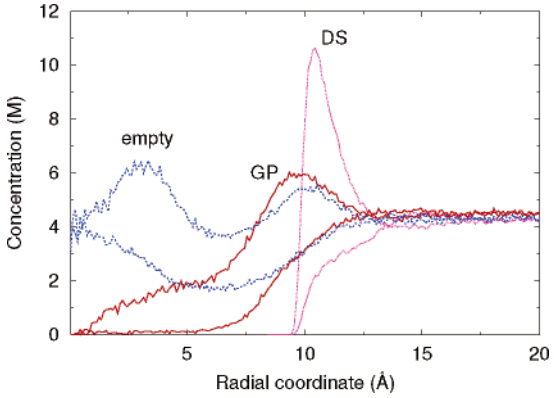

Figure 7. Concentration profiles around Z-DNA at 4.3 M salt concentration. The upper curves are for counterions and the lower ones for coions.

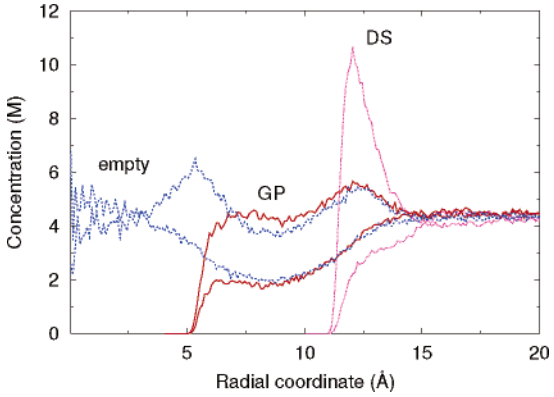

Figure 8. Concentration profiles around B-DNA at 4.3 M salt concentration. The upper curves are for counterions and the lower ones for coions.

Figures 7 and 8 show the concentration profiles for Z- and B-DNA with 4.3 M added salt. The general increase of the ionic concentration profiles with respect to the results at 1 M salt denotes the increase in the salt concentration. In the case of the counterions, the shape of the curves remains essentially the same as in the 1 M systems. The only structurally significant point is that the height of the first maximum of the "empty" model is

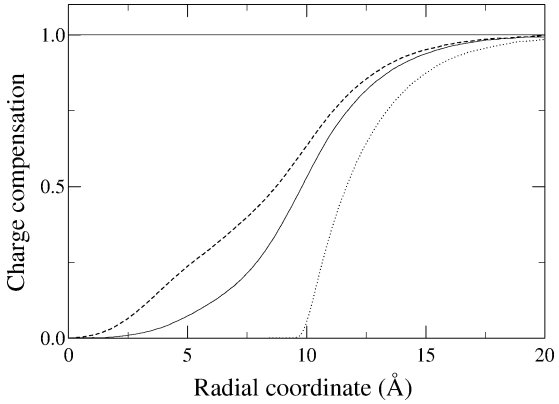

Figure 9. Fraction of the Z-DNA charge compensated by the solution ions for the systems with 1 M added salt. Solid line, GP model; dashed line, "empty" model; dotted line, DS model.

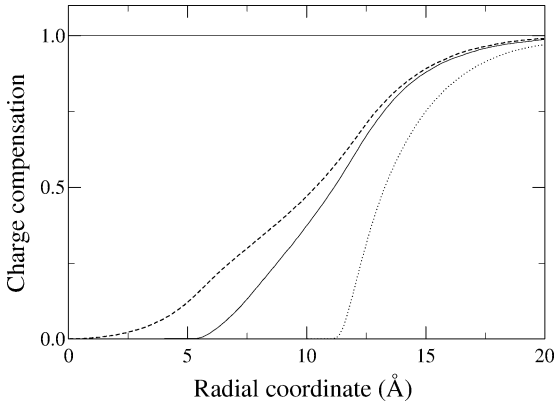

Figure 10. Fraction of the B-DNA charge compensated by the solution ions for the systems with 1 M added salt. Solid line, GP model; dashed line , "empty" model; dotted line, DS model.

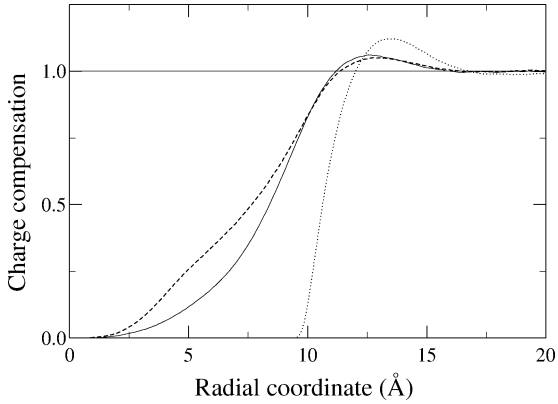

Figure 11. Fraction of the Z-DNA charge compensated by the solution ions for the systems with 4.3 M added salt. Solid line, GP model; dashed line, "empty" model; dotted line, DS model.

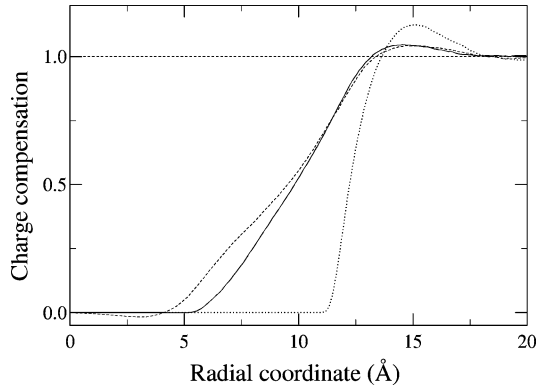

Figure 12. Fraction of the B-DNA charge compensated by the solution ions for the systems with 4.3 M added salt. Solid line, GP model; dashed line, "empty" model; dotted line, DS model.

now of the same order as the second one. The situation is quite different for the coions. The increase in the salt concentration leads to a substantial increment in the number of coions at small radial distances. This is especially noticeable in the "empty" model for which the concentration of coions is the same (or even larger in B-DNA) as that of counterions at the molecular axis. The inner DNA region has enough room that can be occupied by coions because the polyion charge is somewhat shielded by the counterions at the first maximum.

The number of coions in the grooved Z-DNA model at 4.5 M salt (Figure 7) only becomes significant beyond 7.5 Å, just after the position of the more external phosphates (those of type $p = 1$). This is in contrast with B-DNA (Figure 8) for which the coions concentration in the GP model becomes significant at 5−6 Å, i.e., much closer to the DN*A* axis than the phosphates ($\rho = 8.91$ Å). At larger radial coordinates, the coions have similar concentrations in B- and Z-DNA (in fact, it is slightly higher for the latter DNA form). At $\rho = 10$ Å—where the counterions profile of Z-DNA attains its maximum value, 6 M—the coions profile is about 3 M for the GP and "empty" models. Perhaps the more important feature of the concentration profiles of the systems with 4.3 M added salt is the existence of an inversion in the concentration profiles at about 13 Å from the molecular axis. This means that, for all the models, the coions concentration is higher than the counterions concentration. Thus, at such distances, the local net charge has the same sign as DNA.

Figures 9−12show the fraction of DNA charge compensated by the solution ions as a function of the radial distance to the molecular axis for the systems of Figures 5 to 8. At 1 M added salt none of the DNA (B or Z) models yields charge inversion. Nevertheless, all the systems at 4.3 M salt concentration show this peculiar behavior in which the polyion charge is overneutralized at certain distances. The charge inversion is especially prominent in the DS models. The other significant difference between the charge compensation function for the different models is the radial coordinate at which the ions begin to cancel the polyion charge. This reflects the different penetrability of the models. As expected, the charge compensation for the DS model of Z- and B-DNA is null up to values around 10 and 12 Å, respectively, and it increases sharply beyond those radial coordinates, similar to the behavior of the concentration profiles.

It may seem surprising that the charge compensation functions for the "empty" models look relatively similar to that of the corresponding grooved models (especially at the higher salt concentration) despite their differences in the concentration profiles. The cancellation of the DNA charge begins at smaller radial coordinates in the "empty" models but it finally converges to the GP model result. This takes place at distances only slightly beyond the position of the phosphates. In fact, at 4.3 M, the results for the "empty" models are barely distinguishable from those for the grooved model beyond 10 Å. In summary, the structural features observed at distances close to the molecular axis of the "empty" model are considerably blurred in the charge compensation function. The problem is in fact similar to that of the ionic distribution in simple electrolytes.[89,91] The reason for that is quite simple. Although the ionic concentration at small distances from the molecular axis is not negligible, only a low number of ions are involved because of the small value of the concerned volume elements. In this way, such "structural" features are not as relevant as they may appear at first.

Apparently, there are no significant differences between the charge compensation functions for B- and Z-DNA. Indeed, in the three models, the cancellation by the counterions of the Z-DNA charge starts closer to the molecular axis than for B-DNA. But this seems to be a marginal effect as it does not extend to higher radial coordinates. In fact, beyond 7−8 Å from the DNA axis the charge compensation functions of Z- and B-DNA are quite similar. It then can be noticed that the departures between different models of a given DNA form are more significant than the differences between the results for both conformers using the same DNA model representation. In the next section we will see that the relative similarity between the ionic profiles of B- and Z-DNA is due to the averaging over the axial and angular coordinates and that the differences between the spatial distribution of ions for both conformers are important.

2. Deviations from the Cylindrical Symmetry. In this section we present the spatially resolved ionic distribution. As suggested by the results of the previous subsection, the details of the ionic distribution around B-DNA are quite uninteresting for the DS model because the presence of the repulsive cylinder seriously reduces the spatial structuration of ions. In fact, the departures from the cylindrical symmetry in the DS B-DNA model are small and limited to the distances between 10 and 12 Å from the molecular axis.[71] On the other hand, Figures 9−12 show that the differences between the "empty" and the GP models are small and occur mainly in the region of the bases for which the "empty" model results cannot be considered representative. Thus, our discussion will only involve here the ionic spatial distribution for the more realistic of the models presented in the previous section, i.e., the grooved model.

To simplify the description of the spatial distribution of ions we will make use of the helical symmetry of DNA. This reduces the number of coordinates needed to describe the spatial distribution from three to two. We define the hypothetical helix line passing through the external phosphates of chain 1 as the reference helix. The radial distance ρ to the molecular axis remains as one of the coordinates of a given point. To define the other coordinate we first project the point onto the cylinder containing the reference phosphates and calculate either the axial δz or angular $\delta\varphi$ distance to the reference helix line. To evaluate δz one moves from the projected point to the reference helix along a line parallel to the molecular axis. Alternatively, $\delta\varphi$ is obtained by moving from the projected point along the circle normal to the molecular axis until the reference helix is reached. Both definitions are related by $\delta z = (7.43/60)\delta\varphi$—recall that 7.43 Å and 60° are the elevation and rotation, respectively, of the repeating unit in Z-DNA. According to the definition of δz and $\delta\varphi$ their values are restricted to the range 0−44.58 Å (the height of the helix turn) and 0−360°, respectively. A graphical representation of the helical projection is given in ref 71 for B-DNA. Notice that the helical projection implies a small averaging over the spatial ionic distribution because the polyion charge is not uniformly distributed around the reference helix but concentrated on the phosphates. In fact, despite the fact that the phosphates are the center of repulsive sites, it is possible to detect some counterions as placed at the phosphate positions in helical coordinates. They actually correspond to ions placed in the middle of two consecutive phosphates along the reference helix. The effect is more important in Z-DNA than in B-DNA as the rotation between consecutive phosphates is only 36° for the B form. Anyway, rigorous calculations for some test cases indicated to us that the helical averaging does not introduce significant spurious effects while greatly facilitating the analysis, so we stick to the helical projection as presented above.

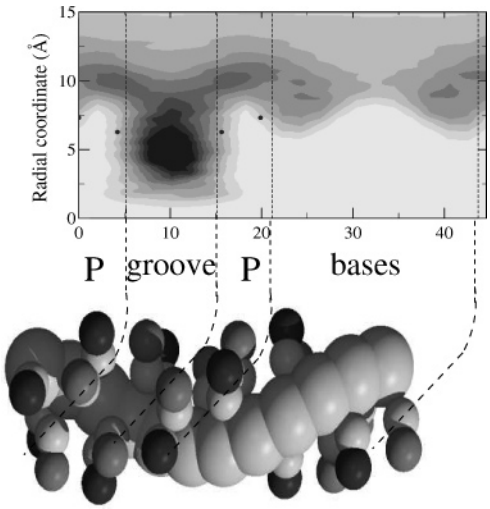

Figure 13. Helical projection of the spatial distribution of counterions at 1 M added salt for the grooved Z-DNA model. The contour plots represent the counterion concentration at a given helical coordinate (δz, ρ), where ρ is the usual radial coordinate (the distance to the molecular axis) and δz is the axial distance to a reference helix defined by the type 1 phosphates of chain 1 (the darker spheres). The gray scale represents 10 concentration ranges from 0 (light gray at the bottom of bases region) to >4.5 M (almost black at the center of the groove). The GP model is represented to facilitate the interpretation of the helical projection. Notice the small filled circles denoting the positions of the four types of phosphates and the dashed−dotted lines delimiting four zones: groove, bases, and two phosphate regions.

The distribution of counterions around Z-DNA at 1 M added salt is shown in Figure 13. We have divided the axial coordinate in four zones denoted as groove region (between 5.2 and 15.1 Å), bases region (from 21.2 to 43.7 Å), and two phosphate regions—one around chain 1 (from −0.88 to 5.2 Å) and the other around chain 2 (from 15.1 to 21.2 Å). Most of the counterion charge is concentrated in the middle of the single DNA groove and closer to the molecular axis than the phosphates. This is a strong signal of a double cooperative effect. First, the phosphates on both sides of the groove create a strong electrostatic field that induces the counterion to being bound at the center of the groove instead of being bound to a given phosphate. On the other hand, the fact that the maximum is reached deep in the groove reflects the influence of the ensemble of the charged phosphates on the other side of DNA. The value of the maximum is of the order of 5 M, about five times larger than the bulk salt concentration. The maximum at the center of the groove splits into two lobes reaching a maximum in the phosphates regions. Those counterions are clearly under the influence of both types of phosphates of a chain as the maxima appear more or less centered between the coordinates of phosphates $p = 1$ and 2. Consequently, there are two maxima, one for each of the chains. In contrast with what happens at the groove region, the maximum is now located outside the Z-DNA molecule, at about 10 Å from its axis. At these positions, the counterion concentration exceeds 3 M. Finally, it should to be noted that the lobes extend along the axial coordinate entering into the bases region where it reaches two new maxima, with concentrations around 2.5 M. They correspond to counterions bound exclusively to one of the external phosphates and placed in the direction opposite to the groove.

The coions distribution for the GP model at 1 M added salt is shown in Figure 14. The spatial distribution of coions is mainly structured along the radial coordinate. A very small

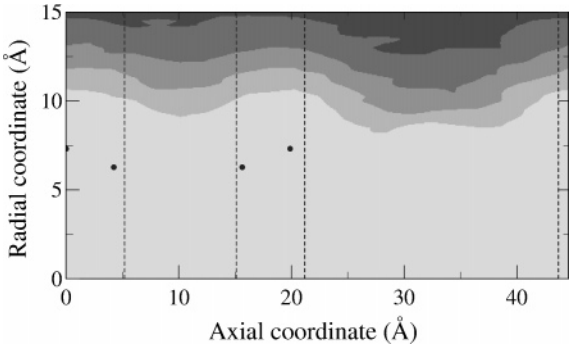

Figure 14. Helical projection of the spatial distribution of coions at 1 M added salt for the grooved Z-DNA model. The gray scale represents five concentration ranges changing from 0−0.2 M (light gray at small radial coordinates) to 0.8−1 M (dark gray at large radial coordinates) at 0.2 M intervals.

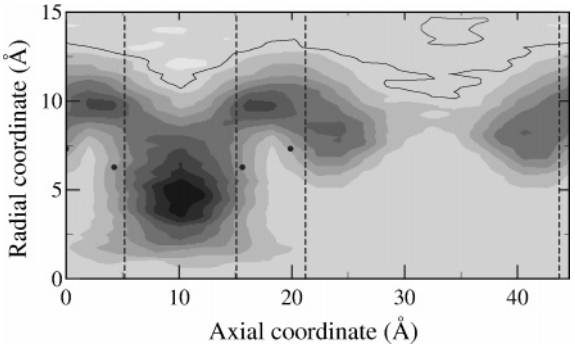

Figure 15. Net charge concentration (counterion minus coion concentration) around the GP Z-DNA model at 4.5 M added salt. The full line is the isoline of zero charge. The gray scale represents concentration ranges in 1 M increments from $c < -0.5$ M (light gray at $\rho \approx 12.5$ Å in the groove region) to $c > 8.5$ M (almost black at the groove).

number of coions approach closer than 9 Å to the Z-DNA axis and the concentration is always null for $\rho < 7$ Å. The concentration of coions increases with the radial distance but it has only slight axial/angular preferences. The highest concentration of coions appears in the bases region, far from the phosphates. There is also a marginally increased concentration at the region of the groove. This is in strong contrast with the situation for B-DNA. There, the coions deeply penetrate into the major groove.[71] The different behavior is determined by the different width of the grooves and the counterions size. In B-DNA, the major groove is wide enough to generate two different lobes of high counterion concentration inside the groove. As a result, the coions may approach these regions of positive charge and become bound in the middle of the lobes just at the groove's limit. These two lobes are also present in Z-DNA but, as the groove is narrower, they appear *outside* the groove and do not induce the approach of coions to the molecular axis. In this way, the single Z-DNA groove behaves much like the minor groove of B-DNA.

From the results at 1 M salt (Figures 13 and 14), it is clear that the net charge concentration around Z-DNA (i.e., the concentration of counterions minus that of coions) looks similar to the counterion distribution presented in Figure 13. The main difference is that, at large distances from the axis, the counterion and coion concentration profiles approach the bulk concentration while the net charge concentration slowly converges to zero. For the system at 1 M salt, the concentration of counterions is always greater than that of coions. At higher added salt concentration the situation is slightly different. At 4.5 M salt, the spatial distributions of counterions and coions follow similar patterns to those at 1 M so we do not present the corresponding plots. But the net charge at 4.5 M salt (Figure 15) shows subtle but significant effects. Obviously, the maxima observed in the counterion distribution give rise to their corresponding maxima for the net charge. Thus, up to 10 Å from the molecular axis the net charge of the mobile ions is positive irrespective of the axial/angular coordinate. Beyond 10−13 Å from the molecular axis the coions concentration exceeds that of counterions (the boundary is the zero charge isoline plotted as a full line in Figure 15). In this way, the local charge in the region beyond the line is negative. Negative values of the net charge were also observed in B-DNA at the same high salt concentration,[71] but do not appear in Z- nor B-DNA at 1 M salt. The regions of local negative charge at 4.5 M salt are different in both conformers. The lighter gray color in Figure 15 corresponds to net charge concentrations below −0.5 M. There is a minimum in front of the single groove at about 12.5 Å from the molecular axis. There is also a less pronounced minimum at the region of the bases

TABLE 4: Net Charge Concentrations at the Maxima and Minima for B- and Z-DNA at 1 and 4.5 M Added Salt Concentration[a]

				charge concn (M)	
type	DNA form	region	number	1 M salt	4.5 M salt
maximum	B	minor groove (inside)	1	4.5	6.2
		major groove (inside)	2	2.9	5.1
		phosphates (binded to)	2	2.4	4.7
	Z	groove (inside)	1	6.7	9.0
		phosphates (binded to)	2	3.2	6.0
		bases (binded to a phosphate)	2	2.4	4.7
minimum	B	major groove (outside)	1		−0.72
		minor groove (outside)	1		−0.72
	Z	groove (outside)	1		−0.85
		bases (outside)	1		−0.36

[a] The column labeled number indicates the number of equivalent extrema in that region.

at 11.5 Å. The value at the minimum is −0.36 M so it has the same color as the surroundings and the minimum cannot be perceived in the figure from 13 to 15 Å. The existence of a very small maximum in the bases region cannot be established unambiguously because of the noise of the simulation results. Despite these small minima, it is to be stressed that, in general, the isoline of zero charge is almost concentric to the Z-DNA axis. This is to be compared with the situation for B-DNA where the region of negative charge is extremely inhomogeneous.[71] There, the radial coordinate at which the charge is negative depends strongly on the axial coordinate: around 7.5 and 12.5 Å, respectively, at the major and minor groove, and beyond 15 Å at the phosphates region.[71] The values of the net charge concentrations at the maxima and minima for B- and Z-DNA at 1 and 4.5 M salt concentration are shown in Table 4. The net charge of the GP models of both B- and Z-DNA DNA show five maxima (in only three nonequivalent positions) and two minima per DNA turn. However, the location of these extrema is completely different for both DNA forms.

Studies dealing with the ionic distribution around Z-DNA are rather scarce. To the best of our knowledge no computer simulations have been reported. The theoretical studies include those of Pack and Klein,[85] Misra and Honig,[38] and Klement et al.[86] The former two papers use the finite difference Poisson−Boltzmann (FDPB) technique. Pack and Klein determined the electrostatic potential for atomic models of B- and Z-DNA at a very low salt concentration, namely, 0.01 M. They modified slightly the FDPB to introduce approximately the finite size of the ions and found a maximum of counterions at the minor

groove of B-DNA and at the single Z-DNA groove, which is in accordance with our results for the GP model. On the other hand, the counterion concentration at the maximum is higher in Z-DNA than in B-DNA, which agrees with the results of this work presented in Table 4. Misra and Honig extended the calculations to the salt concentrations relevant for the study of the B- to Z-DNA transition. They considered the ions as point charges. By introducing a low dielectric constant within DNA they obtained semiquantitative results for the thermodynamics of the transition. However, the structural results are not so good. For example, at 5 M salt the maximum in the counterion profile reaches a value as high as 16 M.[38] It seems that the combination of an atomic description for DNA together with a point charge description for the solution ions is not a satisfactory choice for the calculation of the ionic atmosphere around DNA. Finally, Klement et al.[86] used the Kirkwood superposition approximation together with the exponential mean spherical approximation to evaluate the ionic concentration around B- and Z-DNA. Although the underlying model makes difficult the comparison with the results of the present work it also predicts the maximum of counterions at the center of the Z-DNA groove.

V. Conclusions

In this work we have presented the ionic atmosphere around Z-DNA as yielded by Monte Carlo simulations. Special emphasis is put in the results for a grooved DNA model—described in this work for the first time—as the model combines the approximate DNA shape with the phosphate charges in a simple mesoscopic model. The results indicate that the narrow Z-DNA groove is the preferred location for the counterions as they are stabilized by the surrounding phosphates. Then, the groove behaves very similarly to the minor groove in B-DNA. The coions are completely excluded from the inner molecular regions. This is in contrast with what was observed for B-DNA. The width of the B-DNA major groove allows the accommodation of two counterions (with a similar size as that of the hydrated Na^+ ion) which attract the coions inside the groove yielding a nonnegligible concentration. The maximum in the counterion concentration is higher in Z-DNA than in the B form. Outside the grooves there appear two maxima centered between both types of phosphates, one for each of the chains. And finally, there are two additional maxima in the region of the bases close to the outer phosphates. As in B-DNA, there are also two minima for the net charge due to the accumulation of coions. But contrary to the B-DNA case, the coions concentrate outside the chain, almost concentric to the molecular axis. In summary, both in B-DNA and in Z-DNA we find a structure of alternating positive/negative charges but in Z-DNA the alternation is along the radial coordinate. Notice finally that the structural features are strongly dependent on the accommodation of mobile ions into the groove's structure. For this reason, the spatial distribution of ions depends on the ionic size, which is in accordance with the sensitivity to this parameter of the experimental[101] and computer simulation results[73] of the thermodynamics of the B- to Z-DNA transition.

Despite the extreme simplicity of the "empty" DNA model, its ionic distribution has some similarities with that of the grooved model, especially beyond radial distances of 4−5 Å. On the other hand, the presence of a impenetrable cylindrical core in the DS model disables the structuration of counterions and coions in a similar way. In fact, the radially integrated charge compensation functions of the GP model show a much greater resemblance to those of the "empty" than to the DS model. It is important to note that the predictive ability of the models for the B- to Z-DNA transition is GP > "empty" ≫ DS.[48,72] This seems to confirm that the penetrability of the ions into the grooves (which produces a structure of alternating charges) is essential for the transition to occur. On the other hand, it is to be noticed that the similarities observed in the ionic distributions of the "empty" and GP models are probably linked to the similarities in the results for the B- to Z-DNA transition. In this way the "empty" model not only provides a semiquantitative description of the transition[47,48] but can also serve to improve the results by using the size of the hydrated ions as adjustable parameters as in ref 43.

Acknowledgment. This project has been financed by grants FIS2004-02954-C03-02 of D.G.I. Spain and S-0505/ESP/0299 of the Comunidad de Madrid.

References and Notes

(1) Saenger, W. *Principles of Nucleic Acid Structure;* Springer-Verlag: New York, 1984.
(2) Sinden, R. R. *DNA Structure and Function;* Academic Press: San Diego, CA, 1994.
(3) Groot, L. C. A.; Kuil, M. E.; Leyte, J. C.; van der Maarel, J. R. C.; Cotton, J. P.; Jannink, G. *J. Phys. Chem.* **1994**, *98*, 10167.
(4) Stein, V. M.; Bond, J. P.; Capp, M. W.; Anderson, C. F.; Record, M. T., Jr. *Biophys. J.* **1995**, *68*, 1063.
(5) Manning, G. S. *J. Chem. Phys.* **1969**, *51*, 934.
(6) Bacquet, R. J.; Rossky, P. J. *J. Phys. Chem.* **1984**, *88*, 2660.
(7) Mills, P.; Anderson, C. F.; Record, M. T., Jr. *J. Phys. Chem.* **1985**, *89*, 3984.
(8) Murthy, C. S.; Bacquet, R. J.; Rossky, P. J. *J. Phys. Chem.* **1985**, *89*, 701.
(9) Das, T.; Bratko, D.; Bhuiyan, L. B.; Outhwaite, C. W. *J. Chem. Phys.* **1997**, *107*, 9197.
(10) Gavryushov, S.; Zielenkiewicz, P. *Biophys. J.* **1998**, *75*, 2732.
(11) Outhwaite, C. W.; Bhuiyan, L. B. *J. Chem. Soc., Faraday Trans. 2* **1982**, *78*, 775.
(12) Carnie, S. L.; Torrie, G. M. *Adv. Chem. Phys.* **1984**, *56*, 141.
(13) Gonzales-Tovar, E.; Lozada-Cassou, M.; Henderson, D. *J. Chem. Phys.* **1985**, *83*, 361.
(14) Vlachy, V.; Haymet, A. D. J. *J. Chem. Phys.* **1986**, *84*, 5874.
(15) Strauss, U.; Gershfeld, N. L.; Spiera, H. *J. Am. Chem. Soc.* **1954**, *76*, 5909.
(16) Gil Montoro, J. C.; Abascal, J. L. F. *J. Chem. Phys.* **1995**, *103*, 8273.
(17) Bloomfield, V. A. *Biopolymers* **1991**, *31*, 1471.
(18) Podgornik, R.; Rau, D.; Parsegian, V. *Biophys. J.* **1994**, *66*, 962.
(19) Ha, B.-Y.; Liu, A. J. *Phys. Rev. Lett.* **1997**, *79*, 1289.
(20) Allahyarov, E.; Gompper, G.; Lowen, H. *J. Phys.: Condens. Matter* **2005**, *17*, S1827.
(21) Abascal, J. L. F.; Gil Montoro, J. C. *J. Chem. Phys.* **2001**, *114*, 4277.
(22) Nguyen, T. T.; Rouzina, I.; Shklovskii, B. I. *J. Chem. Phys.* **2000**, *112*, 2562.
(23) Ravindran, S.; Wu, J. Z. *Langmuir* **2004**, *20*, 7333.
(24) Wang, K.; Yu, Y. X.; Gao, G. H. *Phys. Rev. E* **2004**, *70*, 011912.
(25) Pohl, F. M.; Jovin, T. M. *J. Mol. Biol.* **1972**, *67*, 375.
(26) Wang, A. H.-J.; Quigley, G. J.; Kolpak, F. J.; Crawford, J.; van Boom, J. H.; van der Marel, G.; Rich, A. *Nature* (*London*) **1979**, *282*, 680.
(27) Suram, A.; Rao, L. K. S.; Latha, K. S.; Viswamitra, M. A. *NeuroMol. Med.* **2002**, *2*, 289.
(28) Rich, A.; Zhang, S. G. *Nature Rev. Genet.* **2003**, *4*, 566.
(29) Bando, T.; Sugiyama, H. *J. Synth. Org. Chem. Jpn.* **2005**, *63*, 1016.
(30) Rothenburg, S.; Deigendesch, N.; Dittmar, K.; Koch-Nolte, F.; Haag, F.; Lowenhaupt, K.; Rich, A. *Proc. Natl. Acad. Sci. U.S.A.* **2005**, *102*, 1602.
(31) Singleton, C. K.; Klysik, J.; Stirdivant, S. M.; Wells, R. D. *Nature* (*London*) **1982**, *299*, 312.
(32) Peck, L. J.; Nordheim, A.; Rich, A.; Wang, J. C. *Proc. Natl. Acad. Sci. U.S.A.* **1982**, *79*, 4560.
(33) Pohl, F. M. *Cold Spring Harbor Symp. Quantum Biol.* **1983**, *47*, 113.
(34) Frank-Kamenetskii, M. D.; Lukashin, A. V.; Anshelevich, V. V. *J. Biomol. Struct. Dyn.* **1985**, *3*, 35.
(35) Soumpasis, D. M. *J. Biomol. Struct. Dyn.* **1988**, *6*, 563.
(36) Lukashin, A. V.; Beglov, D. B.; Frank-Kamenetskii, M. D. *J. Biomol. Struct. Dyn.* **1991**, *8*, 1113.
(37) Demaret, J.-P.; Guéron, M. *Biophys. J.* **1993**, *65*, 1700.
(38) Misra, V. K.; Honig, B. *Biochemistry* **1996**, *35*, 1115.

(39) Guéron, M.; Demaret, J.-P.; Filoche, M. *Biophys. J.* **2000**, *78*, 1070.
(40) Fenley, M. O.; Manning, G. S.; Olson, W. K. *Biopolymers* **1990**, *30*, 1191.
(41) Gil Montoro, J. C.; Abascal, J. L. F. *Mol. Phys.* **1996**, *89*, 1071.
(42) Henle, M. L.; Santangelo, C. D.; Patel, D. M.; Pincus, P. A. *Europhys. Lett.* **2004**, *66*, 284.
(43) Soumpasis, D. M. *Proc. Natl. Acad. Sci. U.S.A.* **1984**, *81*, 5116.
(44) Hirata, F.; Levy, R. M. *J. Phys. Chem.* **1989**, *93*, 479.
(45) Cherstvy, A. G. *J. Chem. Phys.* **2005**, *123*, 116101.
(46) Gil Montoro, J. C.; Abascal, J. L. F. *Europhys. Lett.* **1996**, *34*, 471.
(47) Gil Montoro, J. C.; Abascal, J. L. F. *J. Chem. Phys.* **1997**, *106*, 8239.
(48) Abascal, J. L. F.; Gil Montoro, J. C. *J. Chem. Phys.* **1999**, *110*, 11094.
(49) Sharp, K. A.; Honig, B. *Curr. Opin. Struct. Biol.* **1995**, *5*, 323.
(50) Anderson, C. F.; Record, M. T., Jr. *Annu. Rev. Phys. Chem.* **1995**, *46*, 657.
(51) Wang, K.; Yu, Y. X.; Gao, G. H.; Luo, G. S. *J. Chem. Phys.* **2005**, *123*, 234904.
(52) Tan, Z. J.; Chen, S. J. *Biophys. J.* **2006**, *90*, 1175.
(53) Jimenez-Angeles, F.; Odriozola, G.; Lozada-Cassou, M. *J. Chem. Phys.* **2006**, *124*, 134902.
(54) Lyubartsev, A. P. In *Dekker Encyclopedia of Nanoscience and Nanotechnology*; Dekker: New York, 2004; p 2131.
(55) Laughton, C. A.; Luque, F. J.; Orozco, M. *J. Phys. Chem.* **1995**, *99*, 11591.
(56) Jayaram, B.; Beveridge, D. L. *Annu. Rev. Biophys. Biomol. Struct.* **1996**, *25*, 367.
(57) Young, M. A.; Jayaram, B.; Beveridge, D. L. *J. Am. Chem. Soc.* **1997**, *119*, 59.
(58) Lyubartsev, A. P.; Laaksonen, A. *J. Biomol. Struct. Dyn.* **1998**, *16*, 579.
(59) Beveridge, D. L.; McConnell, K. J. *Curr. Opin. Struct. Biol.* **2000**, *10*, 182.
(60) Cheatham, T. E., III; Young, M. A. *Biopolymers* **2001**, *56*, 232.
(61) Korolev, N.; Lyubartsev, A. P.; Nordenskiold, L. *Biophys. Chem.* **2003**, *104*, 55.
(62) Várnai, P.; Zakrzewska, K. *Nucleic Acids Res.* **2004**, *32*, 4269.
(63) Rueda, M.; Cubero, E.; Laughton, C. A.; Orozco, M. *Biophys. J.* **2004**, *87*, 800.
(64) Cheng, Y.; Korolev, N.; Nordenskiold, L. *Nucleic Acids Res.* **2006**, *34*, 686.
(65) Long, H.; Kudlay, A.; Schatz, G. C. *J. Phys. Chem. B* **2006**, *110*, 2918.
(66) Drukker, K.; Schatz, G. C. *J. Phys. Chem. B* **2000**, *104*, 6108.
(67) Range, K.; Mayaan, E.; Maher, L. J., III; York, D. M. *Nucleic Acids Res.* **2005**, *33*, 1257.
(68) Sales-Pardo, M.; Guimera, R.; Moreira, A. A.; Widom, J.; Amaral, L. A. N. *Phys. Rev. E* **2005**, *71*, 051902.
(69) Cuesta-Lopez, S.; Errami, J.; Falo, F.; Peyrard, M. *J. Biol. Phys.* **2005**, *31*, 273.
(70) Grandison, S.; Penfold, R.; Vanden-Broecka, J. M. *Phys. Chem. Chem. Phys.* **2005**, *7*, 3486.
(71) Gil Montoro, J. C.; Abascal, J. L. F. *J. Chem. Phys.* **1998**, *109*, 6200.
(72) Abascal, J. L. F.; Gil Montoro, J. C. *J. Phys.*: *Condens. Matter* **2000**, *12*, A327.
(73) Abascal, J. L. F.; Gil Montoro, J. C. *Mol. Phys.* **2004**, *102*, 2141.
(74) Allahyarov, E.; Löwen, H.; Gomper, G. *Phys. Rev. E* **2003**, *68*, 061903.
(75) Allahyarov, E.; Gompper, G.; Lowen, H. *Phys. Rev. E* **2004**, *69*, 041904.
(76) Tan, Z. J.; Chen, S. J. *J. Chem. Phys.* **2005**, *122*, 044903.
(77) Tombolato, F.; Ferrarini, A. *J. Chem. Phys.* **2005**, *122*, 054908.
(78) Haworth, I. S.; Rodger, A.; Richards, W. G. *J. Biomol. Struct. Dyn.* **1992**, *10*, 195.
(79) Eriksson, M. A. L.; Laaksonen, A. *Biopolymers* **1992**, *32*, 1035.
(80) Ohishi, H.; I.; Nakanishi; K.; Tomita. *Biochem. Biophys. Res. Commun.* **1997**, *236*, 146.
(81) Langley, D. R. *J. Biomol. Struct. Dyn.* **1998**, *16*, 487.
(82) Subramanian, P. S.; Beveridge, D. L. *Theor. Chim. Acta* **1993**, *85*, 3.
(83) Kang, N. S.; No, K. T.; Jhon, M. S. *Mol. Simul.* **2003**, *29*, 83.
(84) Gervasio, F. L.; Carloni, P.; M, P. *Phys. Rev. Lett.* **2002**, *89*, 108102.
(85) Pack, G. R.; Klein, B. J. *Biopolymers* **1984**, *23*, 2801.
(86) Klement, R.; Soumpasis, D. M.; Jovin, T. M. *Proc. Natl. Acad. Sci.* **1991**, *88*, 4631.
(87) Wang, A. H.-J.; Quigley, G. J.; Kolpak, F. J.; van der Marel, G.; van Boom, J. H.; Rich, A. *Science* **1981**, *211*, 171.
(88) Rossky, P. J.; Dudowicz, J. B.; Tembe, B. L.; Friedman, H. L. *J. Chem. Phys.* **1980**, *73*, 3372.
(89) Abascal, J. L. F.; Turq, P. *Chem. Phys.* **1991**, *153*, 79.
(90) Vorontsov-Velyaminov, P. N.; Lyubartsev, A. P. *Mol. Simul.* **1992**, *9*, 285.
(91) Abascal, J. L. F.; Bresme, F.; Turq, P. *Mol. Phys.* **1994**, *81*, 143.
(92) Gil Montoro, J. C.; Bresme, F.; Abascal, J. L. F. *J. Chem. Phys.* **1994**, *101*, 10892.
(93) York, D. M.; Darden, T.; Deerfield, D., II; Pedersen, L. G. *Int. J. Quantum Chem., Quantum Biol. Symp.* **1992**, *19*, 145.
(94) Connolly, M. L. *Science* **1983**, *221*, 709.
(95) Sugiyama, H.; Hawai, K.; Matsunaga, A.; Fujimoto, K.; Saito, I. *Nucl. Acid Res.* **1996**, *24*, 1272.
(96) Jovin, T. M.; McIntosh, L. P.; Arndt-Jovin, D. J.; Zarling, D. A.; Robert-Nicoud, M.; van de Sande, J. H.; Jorgenson, K. F.; Eckstein, F. *J. Biomol. Struct. Dyn.* **1983**, *1*, 21.
(97) Brunger, A.; Brooks, C. L.; Karplus, M. *Chem. Phys. Lett.* **1984**, *105*, 495.
(98) Gil Montoro, J. C.; Abascal, J. L. F. *Mol. Simul.* **1995**, *14*, 313.
(99) Brooks, C. L.; Pettitt, B. M.; Karplus, M. *J. Chem. Phys.* **1985**, *83*, 5897.
(100) Guldbrand, L.; Forester, T. R.; Lynden-Bell, R. M. *Mol. Phys.* **1989**, *67*, 473.
(101) Pohl, F. M. *Nature* (*London*) **1976**, *260*, 365.